Title: Experimental considerations for study of *C. elegans* lysosomal proteins

John C. Clancy[1*], An A. Vo[1*], Max T. Levenson[1], James Matthew Ragle[1], and Jordan D. Ward[1‡]

[1]Department of Molecular, Cell, and Developmental Biology, University of California-Santa Cruz, Santa Cruz, CA 95064, USA.

[‡]Author for correspondence.

[*]Equal contribution

Corresponding author email: jward2@ucsc.edu

Keywords: *C. elegans*, lysosome, Gamillus, western blot

Running Title: *C. elegans* lysosome considerations

ABSTRACT

Lysosomes are an important organelle required for the degradation of a range of cellular components. Lysosome function is critical for development and homeostasis as dysfunction can lead to inherited genetic disorders, cancer, and neurodegenerative and metabolic disease. The acidic and protease-rich environment of lysosomes poses experimental challenges. Many fluorescent proteins are quenched or degraded, while specific red fluorescent proteins can be cleaved from translational fusion partners and accumulate. While studying MLT-11, a *C. elegans* molting factor that localizes to lysosomes and the extracellular matrix, we sought to optimize several experimental parameters. We found that mScarlet fusions to MLT-11 missed apical extracellular matrix and rectal epithelial localization in contrast to mNeonGreen fusions. Rapid sample lysis and denaturation was critical for preventing MLT-11 fragmentation while preparing lysates for western blots. Using a model lysosomal substrate (NUC-1) we found that rigid polyproline linkers and truncated mCherry constructs do not prevent cleavage of mCherry from NUC-1. We provide evidence that extended localization in lysosomal environments prevents the detection of FLAG epitopes in western blots. Finally, we optimize an acid-tolerant green fluorescent protein (Gamillus) for use in *C. elegans*. These experiments provide important experimental considerations and new reagents for the study of *C. elegans* lysosomal proteins.

INTRODUCTION

Lysosomes are membrane-enclosed cytoplasmic organelles required for the degradation of diverse biological macromolecules (Ballabio and Bonifacino 2020). Consistent with this function, they are the most acidic compartment in the cell with a pH ranging from 4.5-5.5, and are packed with proteases, nucleases, acid lipases, and carbohydrate processing enzymes (Bonam *et al.* 2019). Lysosome dysfunction can lead to inherited lysosomal storage disorders as well as neurodegenerative and metabolic disease, and cancer (Ballabio and Bonifacino 2020). Lysosome activity declines with age and is required for lifespan extension (Hansen *et al.* 2008; Sun *et al.* 2020).

Using fluorescent protein (FP) fusions to study lysosomal lumenal proteins presents challenges. Many green and red fluorescent proteins derived from avGFP and eqFP578, respectively, are sensitive to degradative lysosomal proteases (Shinoda *et al.* 2018b). The sensitivity of many other FPs to lysosomal proteases remains to be determined (Shinoda *et al.* 2018b). Due to their low pKA (3.1-5.3) and resistance to lysosomal proteases, red FPs derived from DsRed or eqFP611 (ie. mCherry, mScarlet, mRuby) are typically the FP of choice for imaging lysosome lumenal proteins (Shinoda *et al.* 2018b). An additional consideration in interpreting lysosomal localization is that lysosomal proteases can cleave flexible linkers or the N-terminus of fluorescent proteins, separating the FP from the protein of interest (Ko *et al.* 2003; Kollmann *et al.* 2005; Huang *et al.* 2014; Miao *et al.* 2020). While this cleavage can be used to monitor lysosomal activity (Miao *et al.* 2020), it can hamper interpretation of lysosomal localization of fusion proteins. Another issue is that many FPs lose fluorescence in the acidic lysosome through fluorophore quenching due to their neutral pKa (Shinoda *et al.* 2018b). Acid-tolerant green FPs have been recently developed, but have not yet been widely adopted (Roberts *et al.* 2016; Shinoda *et al.* 2018b).

During the course of studying MLT-11, a *C. elegans* protease inhibitor (Ragle et al. 2022), we used CRISPR/Cas9 to introduce an C-terminal mScarlet::3xMyc tag into the endogenous *mlt-11* locus. This strain displayed robust MLT-11::mScarlet::3xMyc lysosomal localization. However, we were unable to verify the fusion was full-length by

anti-Myc western blotting. We also generated an equivalent MLT-11::mNeonGreen::3xFLAG fusion without a linker (Ragle et al. 2022), which displayed similar lysosomal localization, but also transient apical extracellular matrix (aECM) localization. This discrepancy between these strains motivated us to explore whether we could minimize cleavage of the fluorescent protein fusion and explore acid-tolerant green FPs for lysosomal translational fusions.

MATERIALS AND METHODS

Strains and culture

C. elegans were cultured as originally described (Brenner 1974), except worms were grown on MYOB media instead of NGM. MYOB agar was made as previously described (Church *et al.* 1995). We obtained wild type N2 animals from the *Caenorhabditis* Genetics Center.

Strains generated for this study:

Strain	Construction	Genotype
JDW206	CRISPR/Cas9	*mlt-11(wrd41[mlt-11::30x linker-mScarlet^3xMyc])*
JDW254	Crossing	*qxIs630[scav-3::GFP] ; mlt-11(wrd41[mlt-11::30x linker-mScarlet-3xMyc]) V*
JDW288	Microinjection	*wrdEx16[hsp-16.2p::nuc-1::linker::Gamillus::linker::mCherry::tbb-2 3'UTR]*
JDW289	Microinjection	*wrdEx17[hsp-16.2p::nuc-1::linker::Gamillus::linker::mCherry::tbb-2 3'UTR]*
JDW304	Microinjection	*wrdEx20[hsp-16.41p::nuc-1::linker::Gamillus::linker::mScarlet::tbb-2 3'UTR]*

JDW305	Microinjection	*wrdEx21[hsp-16.41p::nuc-1::linker::Gamillus::linker::mScarlet::tbb-2 3'UTR]*
JDW337	Microinjection	*glh-1(wrd65[glh-1::Gamillus]) I*
JDW338	Microinjection	*glh-1(wrd66[GFP::glh-1]) I*
JDW372	CRISPR/Cas9	*his-72(wrd75[his-72::Gamillus] III*
JDW373	CRISPR/Cas9	*lmn-1(wrd76[lmn-1::Gamillus]) I*
JDW391	Ragle et al., 2022	*mlt-11(wrd86[C-terminal mNeonGreen::3xFLAG]) V*
JDW379	RMCE	*jsTi1493 {mosL loxP [wrdSi70(mlt-11p (-2.8 kb)::nuc-1::mCherry-tbb-2 3'UTR)] FRT3::mosR} IV*
JDW382	RMCE	*jsTi1493 {mosL loxP [wrdSi71(mlt-11p (-2.8 kb)::nuc-1::P5::crmCherry::3xFLAG-tbb-2 3'UTR)] FRT3::mosR} IV*

Strains provided by the *Caenorhabditis* Genetics Center:

Strain	Genotype
N2	Wild type
NM5179	*jsTi1493 [mosL loxP mex-5p FLP sl2 mNeonGreen rpl-28p FRT GFP-HIS-58 FRT3 mosR] IV*
XW8056	*qxIs630[scav-3::GFP]*

Molecular biology and generation of transgenic animals

All plasmids used are listed in Table S1. Annotated plasmid sequence files are provided in File S1. Specific cloning details and primers used are available upon request. An *hsp-16.41::linker::Gamillus::linker::mCherry::tbb-2 3'UTR* cassette was synthesized and cloned (Twist Bioscience) to create pJW2138 (Table S1). *nuc-1* coding sequence was Gibson cloned into this vector to create pJW2139 (Table. S1; *hsp-16.41::nuc-*

1::linker::Gamillus::linker::mCherry::tbb-2 3'UTR). This plasmid was injected at 50 ng/µl along with a pCFJ90 (*myo-2p::mCherry*) co-injection marker at 10 ng/µl (Frøkjaer-Jensen *et al.* 2008); two independent lines carrying extrachromosomal arrays were generated (JDW288 and JDW289). The mCherry cassette in pJW2139 was replaced with mScarlet through Gibson cloning to create pJW2145. This plasmid was injected at 50 ng/µl along with a *myo-2p::mCherry* co-injection marker at 5 ng/µl and two independent lines carrying extrachromosomal arrays were generated (JDW304 and JDW305). We used Q5 site-directed mutagenesis (NEB) on pJW2139 to truncate mCherry, remove Gamillus and replace the linker with a rigid penta-proline linker to generate pJW2201. A 3xFLAG tag was added by Gibson cloning to create pJW2204 (Table S1; *hsp-16.41p::nuc-1::P5 linker::crmCherry::tbb-2 3'UTR*). The *nuc-1::P5 linker::crmCherry::3xFLAG::tbb-2 3'UTR* cassette was PCR amplified and ATG and GTA connectors for SapTrap cloning were added (Schwartz and Jorgensen 2016). This PCR product was Gibson cloned to create pJW2325. *nuc-1* and *linker::mCherry::tbb-2 3'UTR* fragments were PCR amplified from pJW2139 and ATG and GTA SapTrap connectors were added (Schwartz and Jorgensen 2016). These products were Gibson cloned to create pJW2322. A 2.8 kb *mlt-11* promoter fragment PCR amplified with SapTrap TGG and ATG connectors and Gibson cloned to generate pJW2286. Integration vectors (pJW2328, pJW2331) for recombination-mediated cassette exchange (RMCE) were created by SapTrap with a pLF3FShC backbone (Schwartz and Jorgensen 2016; Nonet 2020). JDW379 and 382 were created by RMCE using strain NM5179 and pJW2328 and pJW2331, respectively (Nonet 2020).

JDW206 was created using CRISPR/Cas9-mediated genome editing with a pJW1897 repair template and a pJW1896 sgRNA plasmid. Knock-ins were generated and the self-excising cassette was excised as previously described (Dickinson *et al.* 2015). pJW1896 was created by SapTrap using a pJW1839 backbone (Schwartz and Jorgensen 2016; Ashley et al. 2021). pJW1896 was created by SapTrap with 600 bp 5' and 3' homology arms and a pJW1821 (30 amino acid linker::mScarlet (GLO)^SEC Lox511I^3xMyc) cassette (Schwartz and Jorgensen 2016; Ashley *et al.* 2021).

125 **Microscopy**

126 Animals were picked into a 5 µl drop of M9 + 0.05% with levamisole solution on a 2%
127 agarose pad on a microscope slide, then a coverslip was placed on the pad. Images were
128 acquired using a Plan-Apochromat 40x/1.3 Oil DIC lens or a Plan-Apochromat 63x/1.4
129 Oil DIC lens on an AxioImager M2 microscope (Carl Zeiss Microscopy, LLC) equipped
130 with a Colibri 7 LED light source and an Axiocam 506 mono camera. Acquired images
131 were processed through Fiji software (version: 2.0.0- rc-69/1.52p). For direct comparisons
132 within a figure, we set the exposure conditions to avoid pixel saturation of the brightest
133 sample and kept equivalent exposure for imaging of the other samples.

134

135 **Western blotting**

136 For the western blot in Fig. 2, JDW391 animals were synchronized by alkaline bleaching
137 (dx.doi.org/10.17504/protocols.io.j8nlkkyxdl5r/v1) and released on MYOB plates.
138 Animals were harvested at 42 hours post-release by picking thirty animals into 30 µl of
139 M9+0.05% gelatin. Samples were processed as described in Fig 2A. For all other western
140 blots, forty animals were picked into 40 µl of M9+0.05% gelatin and Laemmli sample
141 buffer was added to 1X and then immediately incubated for five minutes at 95ºC. Lysates
142 were then stored at -80ºC until they were resolved by SDS-PAGE. For the western blots
143 in Figure 3, animals were synchronized by bleaching and harvested at the indicated times.
144 Lysates were resolved using precast 4-20% MiniProtean TGX Stain Free Gels (Bio-Rad)
145 with a Spectra™ Multicolor Broad Range Protein Ladder (Thermo; # 26623) protein
146 standard. Proteins were transferred to a polyvinylidene difluoride membrane by semi-dry
147 transfer with a TransBlot Turbo (Bio-Rad). Blots and washes were performed as
148 previously described. Anti-FLAG blots used horseradish peroxidase (HRP) conjugated
149 anti-FLAG M2 (Sigma-Aldrich, A8592-5x1MG, Lot #SLCB9703) at a 1:2000 dilution.

150

151 Mouse anti-alpha-Tubulin 12G10 (Developmental Studies Hybridoma Bank; "-c"
152 concentrated supernatant) was used at 1:4000. Rabbit anti-mCherry (AbCam ab167453)
153 was used at 1:1000. The secondary antibodies were Digital anti-mouse (Kindle
154 Biosciences LLC, R1005) diluted 1:20,000 or Digital anti-Rabbit (Kindle Biosciences LLC,
155 R1006) diluted 1:1000. Blots were incubated for 5 minutes with 1 ml of Supersignal West

156 Femto Maximum Sensitivity Substrate (Thermo Fisher Scientific, 34095) and the final blot
157 were imaged using the 'chemi high-resolution' setting on a Bio-Rad ChemiDoc MP
158 System.
159
160 **Data availability**Strains and plasmids are available upon request. Supplemental files
161 available at FigShare. Plasmid sequences are provided in File S1.

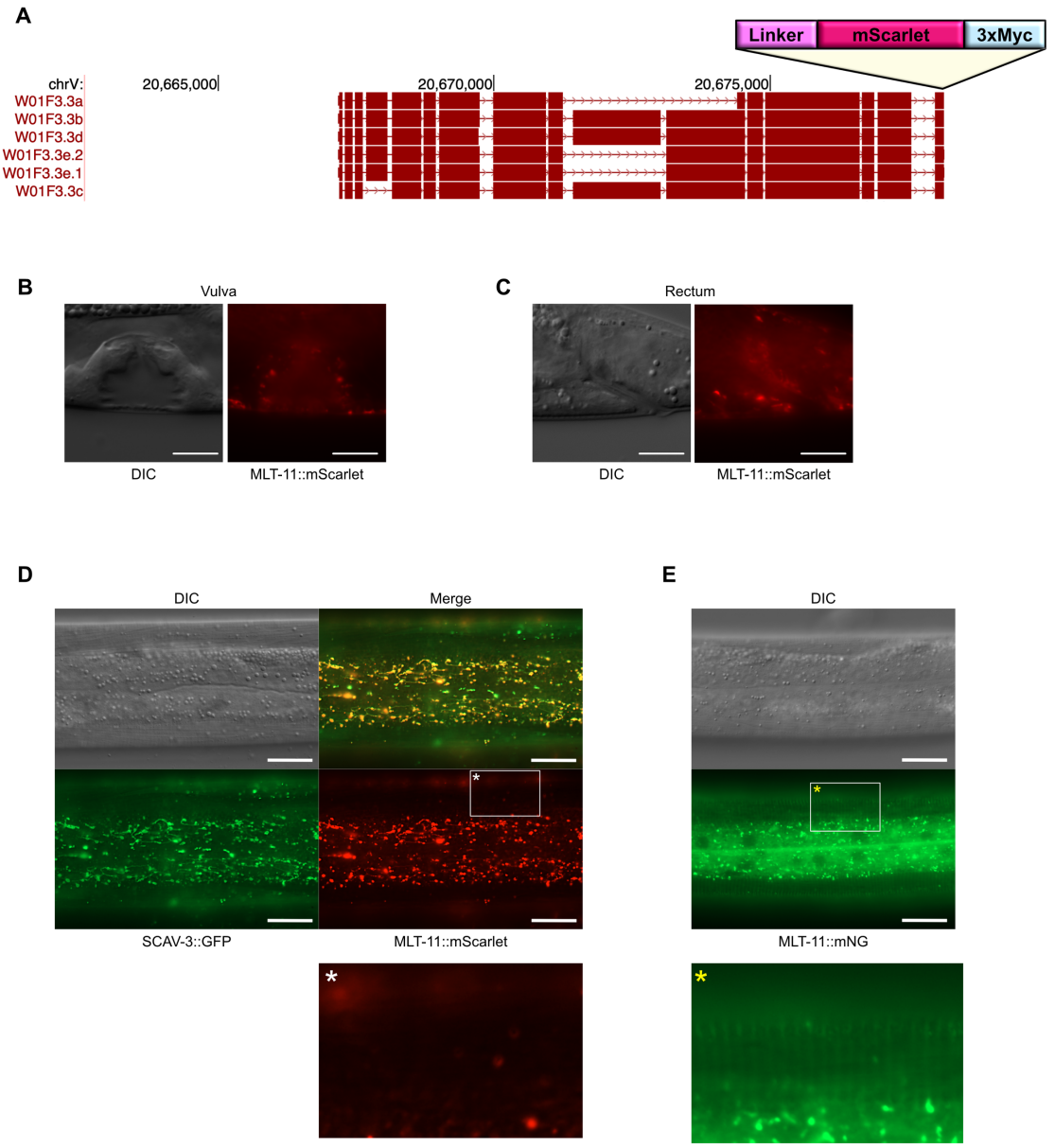

Fig. 1. MLT-11::mScarlet is detected in lysosomes but not the aECM. (A) Representative images of *mlt-11::mScarlet::3xMyc; scav-3::GFP* animals. (B) Representative images of *mlt-11::mNeonGreen::3xFLAG* animals. Scale bars=20 µm. Images are representative of >100 animals examined over four independent experiments.

RESULTS

MLT-11::Scarlet localizes to lysosomes and the vulva but not the aECM or rectal lining

We recently demonstrated that *C. elegans* MLT-11 is an oscillating secreted protein that localizes in the apical ECM and lysosomes (Ragle et al. 2022). Our initial attempts at generating a MLT-11 translational reporter involved inserting an mScarlet::3xMyc cassette with a flexible 30 amino acid linker to C-terminally tag all known *mlt-11* isoforms (Fig. 1A). This knock-in displayed vulval localization (Fig. 1B) similar to the MLT-11::mNeonGreen::3xFLAG (MLT-11::mNG) fusion (Ragle et al. 2022). While we observed MLT-11::mScarlet in rectal epithelial cells (Fig. 1C), we did not observe it lining the rectum as we did for the MLT-11::mNG fusion (Ragle et al. 2022). There was robust MLT-11::mScarlet expression in the hypodermis with a range of expression patterns ranging from punctate to a mesh like network (Fig 1D). This pattern resembled NUC-1::mCherry expression (Miao *et al.* 2020), suggesting MLT-11:mScarlet localized to lysosomes. Accordingly, MLT-11::mScarlet co-localized with the lysosomal marker, SCAV-3::GFP (Fig 1D). We observed a similar lysosomal localization of MLT-11::mNG (Fig. 1E), but also aECM expression that was not observed for MLT-11::Scarlet (Fig. 1D, E). These data highlight that mNG and mScarlet fusions to equivalent positions in a protein can produce different localization patterns.

Sample processing affects MLT-11::mNG stability in lysate generation

As fluorescent tags can be cleaved off fusion proteins in lysosomes (Miao *et al.* 2020), western blotting to confirm that a fusion protein is full-length is essential to have high confidence in lysosomal localization. For our *mlt-11::mScarlet::3xMyc* strain we were never able to detect bands of the predicted size by western blotting with anti-Myc or anti-mScarlet antibodies (unpublished data). When attempting western blots on *mlt-11::mNeonGreen::3xFLAG* lysates we saw variable laddering (for example see Fig 2B, lane C). As lysosomal proteases can degrade proteins, we sought to optimize our sample preparation conditions to minimize degradation. We harvested samples at peak MLT-11 expression (42 hours post-release, stage L4.3 (Mok *et al.* 2015; Ragle *et al.* 2022), and tested a range of variables: i) denaturation at 70ºC for 10 minutes vs 95ºC for 5 minutes

193 ii) denaturing samples immediately after collection vs. rapid freezing and denaturation of
194 all samples together later; iii) rapid freezing using dry ice vs liquid nitrogen; and iv)
195 whether it was better to denature before storage at -80ºC vs denature immediately before
196 resolving samples by SDS-PAGE (Fig. 2A). The best approach was to harvest animals,
197 add Laemmli sample buffer and immediately denature before storage at -80ºC (Fig. 2B
198 lane D and H). Denaturation at 95ºC for 5 minutes produced less laddering than heating

A

Sample	Denaturation	Rapid freezing	Processing
A	70ºC 10 min	Dry ice	Rapid freeze without sample buffer. Store at -80ºC. Add sample buffer while thawing, then denature and resolve by SDS-PAGE
B	70ºC 10 min	Dry ice	Rapid freeze in sample buffer. Denature and store at -80ºC until samples are resolved by SDS-PAGE.
C	70ºC 10 min	Dry ice	Rapid freeze in sample buffer. Store at -80ºC. Thaw and denature, then resolve by SDS-PAGE.
D	70ºC 10 min	None	Add sample buffer and denature immediately. Store at -80ºC until samples are resolved by SDS-PAGE.
E	70ºC 10 min	Liquid nitrogen	Rapid freeze without sample buffer. Store at -80ºC. Add sample buffer while thawing, then denature and resolve by SDS-PAGE
F	70ºC 10 min	Liquid nitrogen	Rapid freeze in sample buffer. Denature and store at -80ºC until samples are resolved by SDS-PAGE.
G	70ºC 10 min	Liquid nitrogen	Rapid freeze in sample buffer. Store at -80ºC. Thaw and denature, then resolve by SDS-PAGE.
H	95ºC 5 min	None	Add sample buffer and denature immediately. Store at -80ºC until samples are resolved by SDS-PAGE.

B

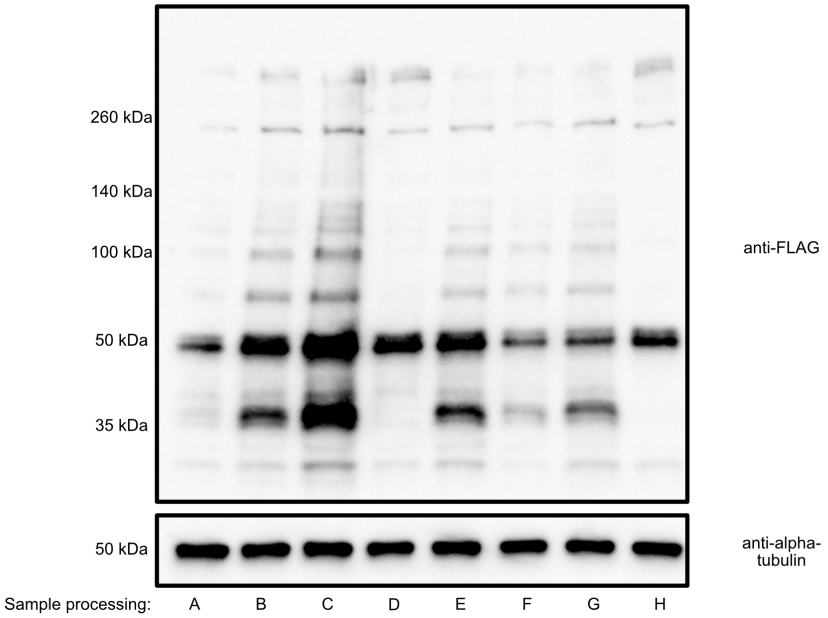

Fig. 2. Immediate denaturation of *mlt-11::mNeonGreen::3xFLAG* samples minimizes degradation. (A) Table describing different sample processing regimens. (B) Anti-FLAG and anti-alpha-tubulin immunoblots on *mlt-11::mNeonGreen::3xFLAG* lysates processed using the conditions described in A. Blot is a representative of two independent experiments.

199 to 70ºC for 10 minutes (Fig 2B compare D to H). The other approaches with various
200 combinations of rapid freezing and denaturation all produced more degradation products
201 above 50 kDa (Fig. 2B). In all conditions there is a strong band at 50 kDa (Fig. 2B),
202 consistent with a C-terminal MLT-11 fragment we previously observed (Ragle et al.,
203 2022). These experiments demonstrate that sample preparation has a significant effect
204 on MLT-11 stability during preparation of lysates for immunoblotting.
205
206 **Proline linkers and truncated mCherry does not reduce tag cleavage**
207 As red FPs are stable in lysosomes and linkers can be cleaved by lysosomal proteases
208 (Shinoda *et al.* 2018b), red FP accumulation might not reflect true localization of a fusion
209 protein. We therefore tested whether we could design FP fusions that underwent minimal
210 cleavage. We used a well-characterized *nuc-1::mCherry* translational fusion as our test
211 case, expressing it in hypodermal and seam cells with a strong *mlt-11* promoter (Ragle
212 et al. 2022). NUC-1::mCherry is cleaved by lysosomal proteases and this cleavage is
213 more frequent when lysosomes acidify during molting (Miao *et al.* 2020). In mammalian
214 cells, rigid linkers comprised of five prolines (P5) helps minimize lysosomal cleavage, as
215 does removing the eleven N-terminal amino acids of mCherry to make a cleavage
216 resistant version (crmCherry)(Huang *et al.* 2014). To test whether these modifications
217 reduce NUC-1::mCherry cleavage in *C. elegans* lysosomes, we generated *mlt-11p::nuc-*
218 *1::P5::crmCherry::3xFLAG* single-copy transgenes. We also generated a *mlt-11p::nuc-*
219 *1::mCherry* strain with the equivalent linker (GGGSRGGTR) used in the *nuc-1::mCherry*
220 constructs of Miao *et al.* (2020). We harvested synchronized mid-L4 larvae, late-L4
221 larvae, and adults for imaging. For both strains, we observed robust lysosomal mCherry
222 at all timepoints (Fig. 3B). We also collected animals for western blot analysis. NUC-
223 1::mCherry and NUC-1::P5::crmCherry::3xFLAG displayed similar punctate and tubular
224 localization at each timepoint (Figure 3B). We observed similar cleavage levels of NUC-
225 1::mCherry and NUC-1::P5::crmCherry::3xFLAG, suggesting that the P5 linker and N-
226 terminal truncation were not effective at preventing cleavage of the mCherry tag (Figure
227 3A). The NUC-1::mCherry control displayed increased cleavage in late-L4 larvae, similar
228 to previous reports (Miao *et al.* 2020). NUC-1::P5::crmCherry::3xFLAG displayed a
229 unique cleavage product compared to NUC-1::mCherry, suggesting that the P5 linker, the

230 N-terminal truncation, and/or the FLAG tag were causing cleavage within NUC-1 (Figure
231 3A).
232

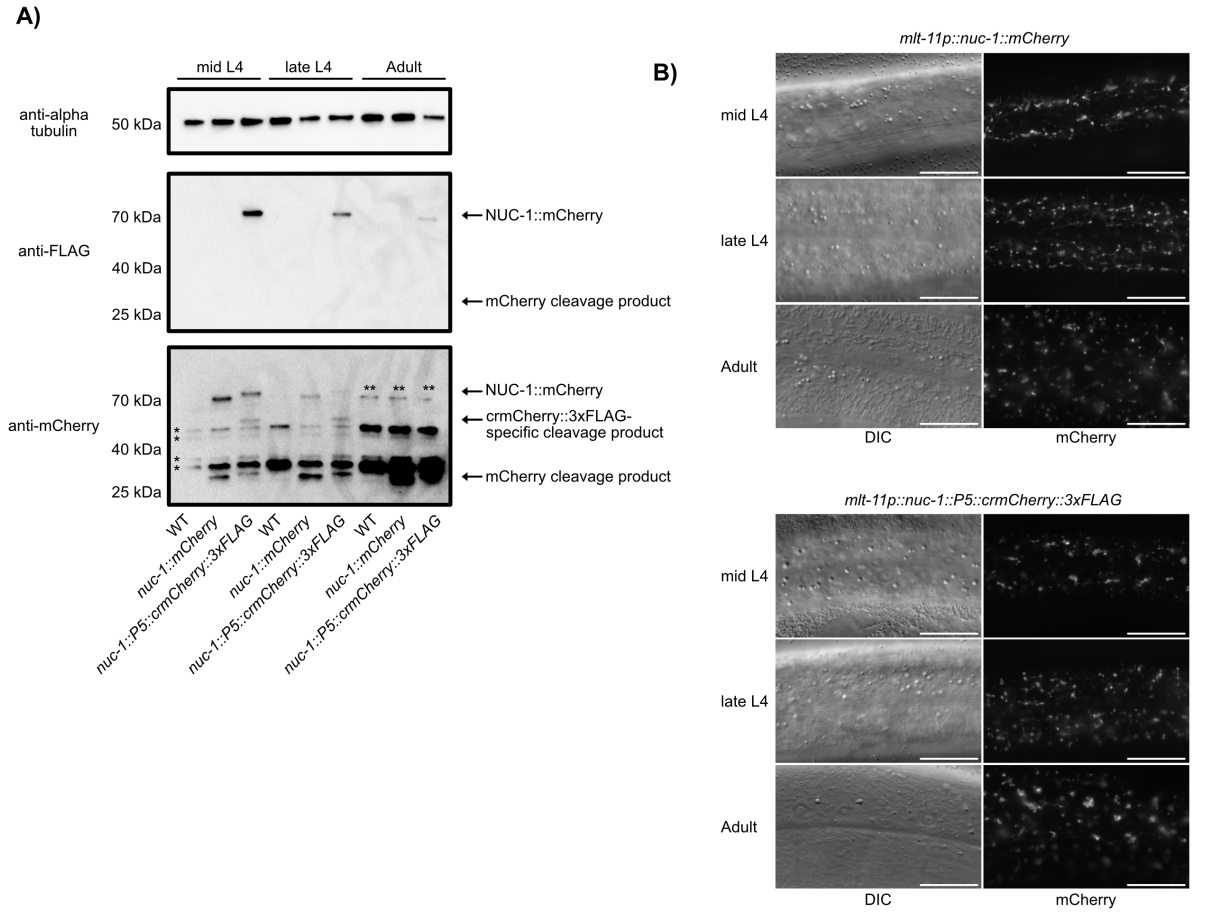

Fig. 3. Rigid proline linkers and truncated mCherry does not prevent cleavage from a NUC-1 fusion. Animals of the indicated genotype were synchronized and harvested in mid L4 (48 hours post-release), late L4 (56 hours post-release), and adulthood (72 hours post-release) for immunoblotting (A) and imaging (B). We performed anti-alpha tubulin, anti-FLAG, and anti-mCherry immunoblots on lysates from the indicated genotypes (A). The blots and images are representative of three experimental replicates. Marker size (in kDa) is provided. Full-length NUC-1::mCherry fusions and cleavage products are indicated by arrows. Non-specific background bands are indicated by asterisks (*). Note that in the adult samples an adult-specific background band not seen in L4 larvae appears. These background bands are indicated by double asterisks (**). (B) Animals of the indicated genotype were imaged at mid L4 and late L4. DIC and mCherry images are provided for each strain and time point. Scale bars=20 µm. Images are representative of 50 animals examined per genotype in two independent experiments.

233

234 **The NUC-1 FLAG epitope is not recognized in immunoblotting after extended time**
235 **in the lysosome**

236 In our FLAG immunoblots, the full-length NUC-1::P5::crmCherry::3xFLAG product
237 declined in intensity in late L4 and adult animals and we did not observe a band at the

238 expected cleavage product position (Fig. 3A). In contrast, in the anti-mCherry
239 immunoblots the cleavage product increased in intensity in late L4 and adult animals. *mlt-*
240 *11* mRNA levels oscillate and the promoter shuts off in mid-L4, so we are monitoring
241 NUC-1::mCherry and NUC-1::P5::crmCherry::3xFLAG produced by the last pulse of gene
242 expression driven by the *mlt-11* promoter (Frand *et al.* 2005; Hendriks *et al.* 2014; Meeuse
243 *et al.* 2020). These data suggest that FLAG epitope is not recognized in the cleaved
244 mCherry fragment, an important consideration in interpreting anti-FLAG immunoblots.
245
246 **The green FP Gamillus is not quenched in *C. elegans* lysosomes**
247 Another limitation of FP usage in lysosomes is that many green FPs are quenched and
248 degraded. The quenching could produce a false negative for lysosomal expression of a
249 fusion protein. As co-localization studies frequently rely on red and green FPs, we sought
250 alternate green FPs for lysosomal imaging. Two candidates from the literature were pH-
251 tdGFP and Gamillus. pH-tdGFP is an engineered tandem dimer which is acid-tolerant and
252 stable *in vitro* over a pH range from 3.75-8.50 (Roberts *et al.* 2016). However, we did not
253 pursue this green FP as the tandem dimer would make it a large insertion for knock-ins
254 which could decrease editing efficiency. Gamillus is an acid tolerant monomeric green FP
255 developed through directed evolution of a novel green FP from the flower hat jellyfish,
256 *Olindias formosa* (Shinoda *et al.* 2018a). It has a pKA of 3.4 and is reported to have
257 desirable brightness, photostability, and maturation speed (Shinoda *et al.* 2018a).
258 Gamillus is photoswitchable; at its peak excitation wavelength of 504 nm it is switched to
259 an off state which could be reversed by irradiation with 352-388 nm light (Shinoda *et al.*
260 2018a). Excitation in the 440-480 nm range produced negligible photochromism,
261 potentially due to a higher on-switching rate (Shinoda *et al.* 2018a).
262
263
264 To test whether Gamillus performs well in *C. elegans* lysosomes, we created a heat
265 shock-inducible *nuc-1::mCherry::Gamillus* transgene. Gamillus and mCherry co-localized
266 in lysosomes 24 hours post-heat shock including in tubular, acidified lysosomes (Figure
267 4A). This result is in contrast to NUC-1::sfGFP::mCherry, where the sfGFP is quenched
268 over time by the acidic lysosomal environment and there is no co-localization 24 hours

269

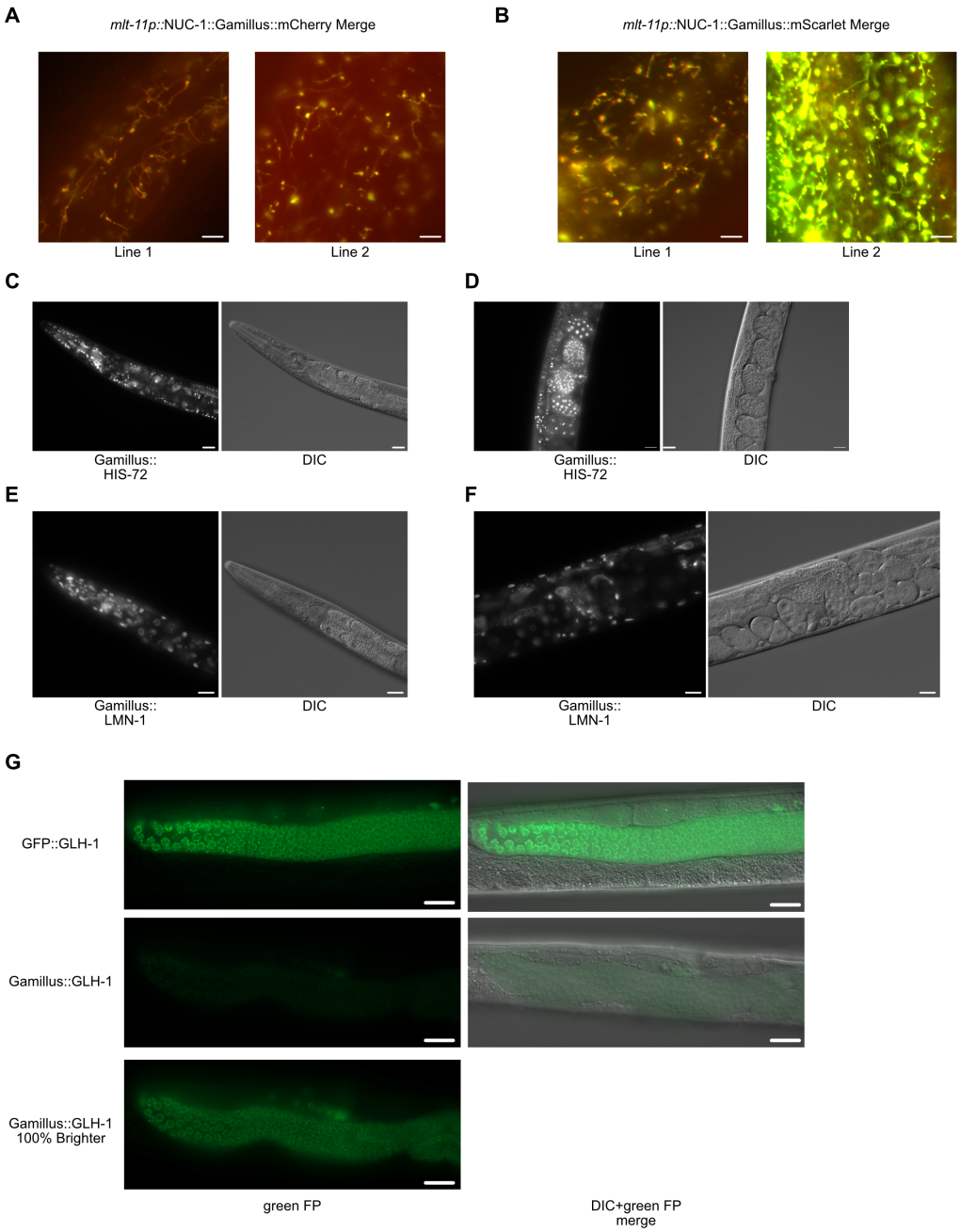

Fig 4. Gamillus is not quenched in lysosomes and does not disrupt localization of *his-72, lmn-1,* and *glh-1* fusion proteins. Mixed stage animals carrying extrachromosomal arrays of *hsp-16.41::nuc-1::Gamillus::mCherry* (A) and *hsp-16.41::nuc-1::Gamillus::mScarlet* (B) were heat-shocked for 30 minutes at 34ºC and adult animals were images 24 hours later. A merge of green and red fluorescent channels is provided. Three biological replicates were performed. Images are representative of 33 animals for JDW288 and JDW304, 49 animals for JDW305, and 8 animals for JDW289. The extrachromosomal array in JDW289 transmits at low rates, hence the lower number of animals scored. Scale bars =5 µm. Gamillus::HIS-72 and DIC image of adult head (C) and embryos (D). Images are representative of 20 animals in two independent replicates. Scale bars=20µm. Gamillus::LMN-1 and DIC image of adult head (E) and embryos (F). Images are representative of 20 animals in two independent replicates. Scale bars=20µm. GFP::GLH-1 and Gamillus::GLH-1 germline images along with DIC overlays (G). A processed Gamillus::GLH-1 image where fluorescence was increased 100% is provided. Scale bars=20µm.

post-heat shock (Miao *et al.* 2020). As the pKa of mScarlet is higher than that of mCherry (pKA 5.3 vs.3.1), we used this approach to test whether mScarlet is quenched by the lysosomal environment. We constructed a heat shock-inducible *nuc-1::mScarlet::Gamillus* and demonstrated that mScarlet and Gamillus also co-localized, suggesting that mScarlet is not quenched or degraded in the lysosome (Figure 4B).

We next tested whether Gamillus affects the function of proteins to which it is fused, using proteins sensitive to tag dimerization. We used CRISPR to knock Gamillus coding sequence into a histone H3B (*his-72*) and lamin *(lmn-1*). We also tagged a germline helicase that localizes to P granules, which are found in ribonucleoprotein condensates. We observed the expected chromatin (*his-72*), nuclear envelope (*lmn-1*), and perinuclear (*glh-1*) localization for each fusion (Figure 4C-G). Notably, Gamillus::GLH-1 knock-ins were dimmer than GFP knock-ins, consistent with the need to image Gamillus at a wavelength that produces 50% excitation to avoid photoconversion (Fig. 4G; Shinoda *et al.* 2018a). These data suggest that Gamillus does not cause mislocalization and validates the FP for tagging proteins by CRISPR-mediated genome editing. Together, these results validate Gamillus as a green FP option for studying lysosome lumenal proteins.

DISCUSSION

Similar to our findings with MLT-11 (Fig. 1; Ragle et al. 2022), different localization patterns of green and red FP fusions have been reported for other *C. elegans* aECM factors such as MLT-10, NOAH-1, and PTR-4 (Meli *et al.* 2010; Cohen *et al.* 2019, 2021; Johnson *et al.* 2022). Lysosomal localization poses different issues for green and red FP fusions. Green FP degradation and/or quenching could create false negatives for lysosomal localization. Conversely, the stability of red FPs in the lysosome could allow a cleaved red FP tag to accumulate in the absence of the fusion protein, creating a false positive for lysosomal localization of a factor of interest. Additionally, the bright lysosomal signal can produce high background, obscuring dimmer localization of a translational fusion of a protein of interest in other tissues or cellular compartments. Determining the extent of FP cleavage by western blotting is a critical control to interpret any lysosomal

301 localization of fusion proteins. Our data also suggest that FLAG epitopes become
302 unrecognizable by anti-FLAG antibodies after extended time in lysosomal environments
303 (Fig. 3). We observed a similar phenomenon with MLT-11::mNeonGreen::3xFLAG where
304 in late L4 larvae and early adulthood we observed lysosomal localization but no signal by
305 anti-FLAG immunoblotting (Ragle *et al.* 2022). These results are likely due to degradation
306 of the epitope by lysosomal proteases, though we cannot rule out post-translational
307 modification of the FLAG tag in the lysosome that prevents antibody binding. Using
308 antibodies against FPs may be preferable to use in immunoblotting as if there is
309 fluorescent signal in animals then one can test whether the fusion protein is full-length.
310 While the rigid proline linker and mCherry N-terminal truncation did not reduce mCherry
311 cleavage from NUC-1, it is possible that they may work on other proteins.
312
313 We also validated Gamillus as a green FP for labeling the lysosome lumen and for fusion
314 to lysosomal proteins. When fused to NUC-1, it displayed similar co-localization and acid-
315 tolerance as mCherry. We also confirmed that despite its higher pKA than mCherry,
316 mScarlet is acid-tolerant making it suitable for lysosomal experiments. Gamillus also
317 exhibits photoswitching behavior at its peak excitation wavelength; however, if non-peak
318 excitation wavelength (440-480 nm) is used the switch to the off-state is minimized at the
319 cost of brightness (Shinoda *et al.* 2018a).
320
321 **ACKNOWLEDGEMENTS**
322 We thank D. Kellogg for helpful discussions. This work was funded by the National
323 Institutes of Health (NIH) National Institute of General Medical Sciences (NIGMS) [R01
324 GM138701] to J.D.W. Some strains were provided by the Caenorhabditis Genetics
325 Center, which is funded by the NIH Office of Research Infrastructure Programs [P40
326 OD010440]. The anti-alpha tubulin 12G10 monoclonal antibody developed by J. Frankel
327 and E.M. Nelson of the University of Iowa was obtained from the Developmental Studies
328 Hybridoma Bank, created by the NICHD of the NIH and maintained at The University of
329 Iowa, Department of Biology, Iowa City, IA 52242.
330
331

REFERENCES

Ashley, G. E., T. Duong, M. T. Levenson, M. A. Q. Martinez, L. C. Johnson *et al.*, 2021 An expanded auxin-inducible degron toolkit for *Caenorhabditis elegans*. Genetics 217: iyab006.

Ballabio, A., and J. S. Bonifacino, 2020 Lysosomes as dynamic regulators of cell and organismal homeostasis. Nat. Rev. Mol. Cell Biol. 21: 101–118.

Bonam, S. R., F. Wang, and S. Muller, 2019 Lysosomes as a therapeutic target. Nat. Rev. Drug Discov. 18: 923–948.

Brenner, S., 1974 The genetics of *Caenorhabditis elegans*. Genetics 77: 71–94.

Church, D. L., K. L. Guan, and E. J. Lambie, 1995 Three genes of the MAP kinase cascade, *mek-2*, *mpk-1/sur-1* and *let-60 ras*, are required for meiotic cell cycle progression in *Caenorhabditis elegans*. Development 121: 2525–2535.

Cohen, J. D., C. E. Cadena del Castillo, N. D. Serra, A. Kaech, A. Spang *et al.*, 2021 The *Caenorhabditis elegans* Patched domain protein PTR-4 is required for proper organization of the precuticular apical extracellular matrix. Genetics.

Cohen, J. D., K. M. Flatt, N. E. Schroeder, and M. V. Sundaram, 2019 Epithelial Shaping by Diverse Apical Extracellular Matrices Requires the Nidogen Domain Protein DEX-1 in *Caenorhabditis elegans*. Genetics 211: 185–200.

Dickinson, D. J., A. M. Pani, J. K. Heppert, C. D. Higgins, and B. Goldstein, 2015 Streamlined Genome Engineering with a Self-Excising Drug Selection Cassette. Genetics 200: 1035–1049.

Frand, A. R., S. Russel, and G. Ruvkun, 2005 Functional Genomic Analysis of *C. elegans* Molting. PLoS Biol. 3: e312.

Frøkjaer-Jensen, C., M. W. Davis, C. E. Hopkins, B. J. Newman, J. M. Thummel *et al.*, 2008 Single-copy insertion of transgenes in *Caenorhabditis elegans*. Nat. Genet. 40: 1375–1383.

Hansen, M., A. Chandra, L. L. Mitic, B. Onken, M. Driscoll *et al.*, 2008 A role for autophagy in the extension of lifespan by dietary restriction in *C. elegans*. PLoS Genet. 4: e24.

Hendriks, G.-J., D. Gaidatzis, F. Aeschimann, and H. Großhans, 2014 Extensive oscillatory gene expression during *C. elegans* larval development. Mol. Cell 53:

380–392.

Huang, L., D. Pike, D. E. Sleat, V. Nanda, and P. Lobel, 2014 Potential Pitfalls and Solutions for Use of Fluorescent Fusion Proteins to Study the Lysosome. PLOS ONE 9: e88893.

Johnson, L. C., A. A. Vo, J. C. Clancy, J. D. Aguilera, M. T. Levenson *et al.*, 2022 NHR-23 activity is necessary for developmental progression and apical extracellular matrix structure and function. 2021.10.27.465992.

Ko, D. C., J. Binkley, A. Sidow, and M. P. Scott, 2003 The integrity of a cholesterol-binding pocket in Niemann-Pick C2 protein is necessary to control lysosome cholesterol levels. Proc. Natl. Acad. Sci. U. S. A. 100: 2518–2525.

Kollmann, K., K. E. Mutenda, M. Balleininger, E. Eckermann, K. von Figura *et al.*, 2005 Identification of novel lysosomal matrix proteins by proteome analysis. Proteomics 5: 3966–3978.

Meeuse, M. W., Y. P. Hauser, L. J. Morales Moya, G. Hendriks, J. Eglinger *et al.*, 2020 Developmental function and state transitions of a gene expression oscillator in *Caenorhabditis elegans*. Mol. Syst. Biol. 16:.

Meli, V. S., B. Osuna, G. Ruvkun, and A. R. Frand, 2010 MLT-10 Defines a Family of DUF644 and Proline-Rich Repeat Proteins Involved in the Molting Cycle of *Caenorhabditis elegans*. Mol. Biol. Cell 21: 1648–1661.

Miao, R., M. Li, Q. Zhang, C. Yang, and X. Wang, 2020 An ECM-to-Nucleus Signaling Pathway Activates Lysosomes for *C. elegans* Larval Development. Dev. Cell 52: 21-37.e5.

Mok, D. Z. L., P. W. Sternberg, and T. Inoue, 2015 Morphologically defined sub-stages of *C. elegans* vulval development in the fourth larval stage. BMC Dev. Biol. 1–8.

Nonet, M. L., 2020 Efficient Transgenesis in *Caenorhabditis elegans* Using Flp Recombinase-Mediated Cassette Exchange. Genetics 215: 903–921.

Ragle, J. M., M. T. Levenson, J. C. Clancy, A. A. Vo, V. Pham *et al.*, 2022 The conserved, secreted protease inhibitor MLT-11 is necessary for *C. elegans* molting and embryogenesis. 2022.06.29.498124.

Roberts, T. M., F. Rudolf, A. Meyer, R. Pellaux, E. Whitehead *et al.*, 2016 Identification and Characterisation of a pH-stable GFP. Sci. Rep. 6: 28166.

394 Schwartz, M. L., and E. M. Jorgensen, 2016 SapTrap, a Toolkit for High-Throughput
395 CRISPR/Cas9 Gene Modification in *Caenorhabditis elegans*. Genetics 202:
396 1277–1288.
397 Shinoda, H., Y. Ma, R. Nakashima, K. Sakurai, T. Matsuda *et al.*, 2018a Acid-Tolerant
398 Monomeric GFP from *Olindias formosa*. Cell Chem. Biol. 25: 330-338.e7.
399 Shinoda, H., M. Shannon, and T. Nagai, 2018b Fluorescent Proteins for Investigating
400 Biological Events in Acidic Environments. Int. J. Mol. Sci. 19:.
401 Sun, Y., M. Li, D. Zhao, X. Li, C. Yang *et al.*, 2020 Lysosome activity is modulated by
402 multiple longevity pathways and is important for lifespan extension in *C. elegans*.
403 eLife 9: e55745.
404
405
406
407
408
409
410
411
412
413
414